OPTIMIZING RF LINACS AS DRIVERS FOR INVERSE COMPTON SOURCES: THE ELI-NP CASE

C. Vaccarezza, D. Alesini, M. Bellaveglia, R. Boni, E. Chiadroni, G. Di Pirro, M. Ferrario,
A. Gallo, G. Gatti, A. Ghigo, B. Spataro, P. Tomassini, INFN-LNF, Frascati, Italy
A. Bacci, I. Drebot, D. Palmer, V. Petrillo, A. R. Rossi, L. Serafini, , INFN-MI, Milano, Italy
A. Giribono, A. Mostacci, L. Palumbo, University of Rome La Sapienza , Italy
A. Cianchi, University of Rome Tor Vergata, Italy
C. Ronsivalle, ENEA-CRE, Frascati, Italy

Abstract

The design guide-lines of RF Linacs to fulfil the requirements of high spectral density Inverse Compton Sources for the photo-nuclear science are mostly taken from the expertise coming from high brightness electron Linacs driving X-ray FEL's. The main difference is the quest for maximum phase space density (instead of peak brightness), but many common issues and techniques are exploited, in order to achieve an optimum design and lay-out for the machine. A relevant example in this field is the design of the hybrid C-band multi-bunch RF Linacs for the ELI-NP Gamma Beam System, aiming at improving by two orders of magnitude the present state of the art in spectral density available for the gamma-ray beam produced.

INTRODUCTION

In the last two decades the crucial role played by the high brightness electron beams in the frontier fields of radiation generation and advanced acceleration schemes has been largely established. The production of high quality phase space electron beams has shown to be essential for the coherent X-rays generation in the FEL's as well to provide the matching conditions for the novel acceleration schemes based on high gradient wakefields and for the realization of bright Gamma-ray Compton sources. The characteristic brightness parameter B can be expressed as:

$$B = \frac{2I}{\epsilon_n^2} \qquad (1)$$

where I (A) is the beam current and ε_n is the normalized emittance in the transverse phase space, hence high brightness means high current and a small footprint in the transverse phase space. A big effort has been devoted in these years to develop fruitful techniques of phase space control and manipulation of intense electron sources based on RF guns, equipped with laser driven photocathodes, followed by one or two accelerating sections (photoinjectors). The proper shaping of the laser pulse hitting the photocathode has been intensely studied together with the apposite properties of accelerating and focusing field in the gun and in the downstream linac sections as well.

In the first section of this paper the main aspects of the high brightness beam production in a photoinjector will be described while in the following section the phase space density optimization will be described for the ELI case. In the third section the ELI-NP Gamma Beam System design will be illustrated.

THE HIGH BRIGHTNESS BEAM EXPERIENCE

The Photoinjector Optimization

A simple emittance compensation scheme [1] based on a focusing solenoid at the exit of the RF gun, can be used in photoinjectors to control emittance growth due the space charge effects while, from the invariant envelope theory [2], a proper matching of the transverse space of the electron beam injected in the downstream accelerating sections (booster) after the gun exit can help to control the transverse emittance oscillations during the acceleration. It is shown in the paper that in the space charge dominated regime these oscillations are due to the mismatch between the space charge correlated forces and the rf focusing gradient, and to dump these oscillations the beam has to be injected into the booster under the invariant envelope condition, i.e. at the laminar envelope waist occurrence ($\sigma' = 0$), while the following condition has to be fulfilled for the accelerating gradient E_{acc}:

$$\gamma' = \frac{2}{\sigma}\sqrt{\frac{\hat{I}}{2I_0\gamma}}, \qquad (2)$$

where $\gamma' \approx 2E_{acc}$, σ is the transverse rms beam size, $\hat{I}$ is the peak current, I_o=17kA is the Alfven current, and γ is the beam energy. In this way the damping of the emittance oscillations is provided but its final value at the linac exit depends on the phase of the plasma oscillations at the entrance of the booster that has to be located at a relative emittance maximum occurrence [3] in order to shift the following emittance minimum at higher energy where, taking advantage of the additional emittance compensation due to the booster, the emittance can be frozen at its lowest value at the exit of the linac. Under the conditions of invariant envelope and proper phasing of space charge oscillations [4] the final emittance is almost compensated down to the thermal emittance value given by cathode emission with an expected emittance

scaling like $\varepsilon_n \propto \sigma_{cath.} \propto Q^{1/2}$, where ε_n is the normalized transverse emittance, $\sigma_{cath.}$ the hitting laser spotsize on the photocathode, and Q the extracted electron charge.

The Bunch Compression

To achieve the high peak currents required by several applications such as short wavelengths free electron lasers, plasma wake field accelerators, and so on a compression stage is necessary; the magnetic compressors are largely adopted for this purpose, however another method, i.e. the velocity bunching [5], can be adopted and integrated in the emittance compensation process [6] to provide the desired control of the emittance growth with the advantage of compactness of the machine and absence of Coherent Synchrotron Radiation (CSR) effects [7].

This well-known compression process consists in a rotation of the longitudinal electron phase space based on a time-velocity correlation (chirp) for which the electrons in the bunch tail are faster than those in the bunch head. This happens in the longitudinal potential of a travelling wave accelerating structure that accelerates the beam and at the same time applies an off crest energy chirp when the injected beam is slightly slower than the phase velocity of the rf wave, in such a way that when injected at the zero crossing field phase it slips back to accelerating phases.

The electron beam is then compressed and accelerated at the same time in the first accelerating section after the rf gun and, under the above described conditions of invariant envelope and proper phasing of space charge oscillations, it is possible to keep control of the emittance growth. In reference [8] the first experimental results obtained at SPARC are reported of velocity bunching compression with applied optimized compensation resulting in a significant mitigation of the emittance growth due to the compression process.

THE ELI-NP GBS RF LINAC DESIGN

The ELI-NP Gamma Beam System (GBS) is an advanced Gamma-ray Source project planned to produce beams of monochromatic and high spectral density gamma photons, up to two orders of magnitude better than the present state of the art [9,10,11]. The GBS is based on a Compton back scattering source with photon energy tunable in the range 1-20 MeV, rms bandwidth smaller than 0.5%, spectral density larger than 10^4 photons/sec·eV, and a peak brilliance for the gamma beam larger than 10^{20} photons/(sec.mm^2.mrad^2.0.1%), see Table 1. The Compton back scattering collision process, depicted in Fig. 1, between a relativistic electron bunch and a high power laser can be described in terms of luminosity as for a collider:

$$L = \frac{N_{el}N_{las}}{2\pi\left(\sigma_x^2 + \frac{w_0^2}{4}\right)} f \cdot n_{RF} \cdot \delta_\phi, \quad (3)$$

Table 1: ELI-NP Gama Beam system specifications

|		
Photon energy	*MeV*	0.2-19.5
Spectral Density	*ph/sec.eV*	0.8-4·10^4
Bandwidth (rms)	*%*	$\leq$0.5
# photons per shot within FWHM bdw.		$\leq$2.6·10^5
# photons/sec within FWHM bdw.		$\leq$8.3·10^8
Source rms size	*μm*	10 - 30
Source rms divergence	*μrad*	25 - 200
Peak Brilliance (N_{ph}/sec·mm^{2}mrad^2·0.1%)		10^{20} - 10^{23}
Radiation pulse length	(rms, *psec*)	0.7 - 1.5
Linear Polarization	*%*	> 99
Macro rep. rate	*Hz*	100
# of pulses per macropulse		$\leq$32
Pulse-to-pulse separation	*nsec*	16
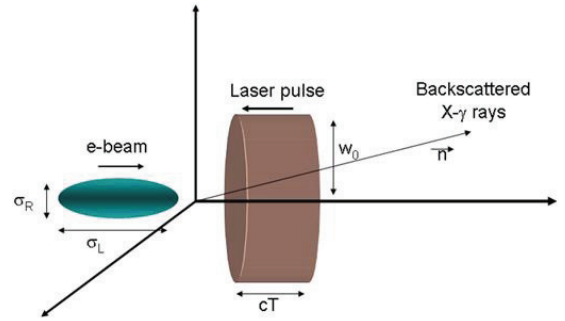
Figure 1: Compton/Thomson backscattering geometry. The electron beam of longitudinal and transverse sizes σ$_L$ and σ$_R$ respectively, is moving at a relativistic speed from left to right, colliding with a photon beam of waist size w$_0$ and duration T, thus emitting scattered radiation mainly in the direction of motion of the electron beam.pulse.

Where N_{el} is the number of electrons in the electron bunch, N_{Las} is the number of optical photons in the laser, σ_x is the rms electron spot size, under the assumption of round beams ($\sigma_x = \sigma_y$), w_0 is the laser beam waist, f is the collision repetition rate defined as $f = f_{RF}n_{RF}$, being f_{RF} the RF repetition rate and n_{RF} the number of bunches in each RF pulse, and δ_ϕ is the correction factor due to a non-zero collision angle. The flux $N_\gamma(photons \cdot s)$ is simply :

$$N_\gamma = \Sigma_{TH}L, \quad (4)$$

where $\Sigma_{TH} = 0.67 \times 10^{-24} cm^2$ is the Thomson cross-section. In a more practical notation the above equation can be expressed in terms of the energy carried by the laser U_L, and the electron bunch charge Q:

$$N_\gamma = 4.2 \times 10^8 \frac{U_L[J]Q[pC]f\, n_{RF}\, \delta_\phi}{h\nu[eV]\left(\sigma_x^2[\mu m]+\frac{w_0^2[\mu m]}{4}\right)} \quad (5)$$

where $h\nu = 2.4\,eV$, and for the ELI-NP GBS typical values of $Q = 250\,pC$, $U_L = 0.4\,J$, an interaction spot size $\sigma_x \approx 15\,\mu m$, and a laser beam waist $w_0 \approx 28\,\mu m$, gives a gamma ray flux of $N_\gamma \approx 3 \times 10^9 s^{-1}$ over the entire solid angle at $f = 100\,Hz$.

What is interesting, however, is the number of photons emitted in the desired bandwidth bw, that scales nearly like the square of the normalized collimation angle $bw \approx \gamma^2\theta^2$, and for the number of photons emitted in a collimation angle θ we can write:

$$N_\gamma^{bw} = 1.4 \times 10^9 \frac{U_L[J]Q[pC]f\, n_{RF}\, \delta_\phi}{h\nu[eV]\left(\sigma_x^2[\mu m]+\frac{w_0^2[\mu m]}{4}\right)} \cdot$$
$$\sqrt{\left(\frac{\Delta\nu_\gamma}{\nu_\gamma}\right)^2 - \left(2\frac{\Delta\gamma}{\gamma}\right)^2 - \left(\frac{2\varepsilon_n^2}{\sigma_x^2}\right)^2 - \left(\frac{\Delta\nu}{\nu}\right)^2 - \left(\frac{M^2\lambda_L}{2\pi w_0}\right)^4 - \left(\frac{a_0^2/3}{1+a_0^2/2}\right)^2} \quad (6)$$

More in detail the frequency ν_γ of the radiation emitted within a small angle of scattering and electron incidence θ_c around the propagation axis of the electron beam is given by:

$$\nu_\gamma = \nu_L \frac{4\gamma^2}{1+\gamma^2\theta_c^2+a_0^2/2}(1-\Delta) \quad (7)$$

where ν_L is the laser optical frequency, a_0 the laser parameter and the dimensionless parameter $\Delta = \frac{4\gamma h\nu_L/mc^2}{1+2\gamma h\nu_L/mc^2}$ represents the red-shift due to the electron recoil; the rms bandwidth of the gamma ray beam, deduced from the Compton relation [12,13], scales with the quadratic sum of the contributions due respectively to the normalized collimation angle, or acceptance $\Psi = \gamma\theta$, the normalized transverse emittance ε_n, the laser natural bandwidth, diffraction and temporal profile, similar to the corresponding classical terms:

$$\frac{\Delta\nu_\gamma}{\nu_\gamma} \cong$$
$$\sqrt{\left(\frac{\gamma^2\theta^2}{2}\right)^2 + \left(2\frac{\Delta\gamma}{\gamma}\right)^2 + \left(\frac{2\varepsilon_n^2}{\sigma_x^2}\right)^2 + \left(\frac{\Delta\nu}{\nu}\right)^2 + \left(\frac{M^2\lambda_L}{2\pi w_0}\right)^4 + \left(\frac{a_0^2/3}{1+a_0^2/2}\right)^2}, (8)$$

where in the last three terms all the contributions coming from the laser are taken into account.

The spectral density is defined as :

$$S \equiv \frac{N_\gamma^{bw}}{\sqrt{2\pi}h\Delta\nu_\gamma} \quad (9)$$

that once the required bandwith value $\left[\Delta\nu_\gamma/\nu_\gamma\right]_r$ has been fixed from the source design becomes:

$$S_r(eV^{-1}) = \frac{0.35\times10^9 E_L Q\Psi^2}{h\omega\nu_L\left(\sigma_x^2+\frac{w_0^2}{4}\right)} \frac{1}{\sqrt{2\pi}h\Delta\nu_\gamma\left[\frac{\Delta\nu_\gamma}{\nu_\gamma}\right]_r}. \quad (10)$$

Looking at the above equation the best photo-linac for such a Compton source turns out to be the one providing for the electron beam the maximum value of the parameter $\frac{Q}{\sigma_x^2[\Delta\gamma/\gamma+(2\varepsilon_n/\sigma_x)^2]}\,[photons/sec/eV]$.

As pointed out in [10] in a high brightness photo-linac the longitudinal and transverse space are handled in uncoupled way especially if no further bunch compression is needed, as in the ELI case, so it can be assumed that the transverse emittance can be minimized independently on the beam energy spread, and the qualifying parameter for such a photo-linac is instead the 4-D transverse space density:

$$\eta \equiv \frac{Q}{\epsilon_n^2}. \quad (11)$$

From the above considerations it follows that the maximum spectral density of the gamma ray beam is reached for the maximum transverse space density of the electron beam.

The ELI-NP GBS requirements of a spectral density $>10^4$ ph/sec/eV in a narrow rms bandwidth $<0.3\%$ corresponds to an electron beam with energy spread $<0.1\%$ and a phase space density $\eta = Q/\epsilon_n^2 > 10^3$.

Despite the FEL case were a high brightness beam and a minimum slice emittance are required, in the high phase density case the required minimum of the projected emittance can be achieved only with a long enough electron beam pulse, i.e. at expenses of the final energy spread, due to the RF curvature, while on the other side the reduction of the energy spread by means of a short electron pulse production from the cathode leads to an irreversible growth of the transverse emittance.

The solution proposed for the ELI-NP GBS [9] foresees a long enough electron beam pulse from the photocathode to control the emittance, and a velocity bunching compression stage in the very next accelerating section to compress the beam and reduce the energy spread, namely a hybrid layout made of a SPARC-like S-band photoinjector [17] followed by a C-band RF linac, as described in the following section, and which parameter list is reported in Table 2.

THE ELI-NP GBS LAYOUT

The ELI-NP GBS consists in a S-band photoinjector followed by a RF Linac operated at C-band (5.7 GHz), and it is meant to deliver a high phase space density electron beam in the 250-720 MeV energy range.

Two interaction points are foreseen where the collision

Table 2: ELI_NP GBS Electron beam parameters at the Interaction Points (rms values)

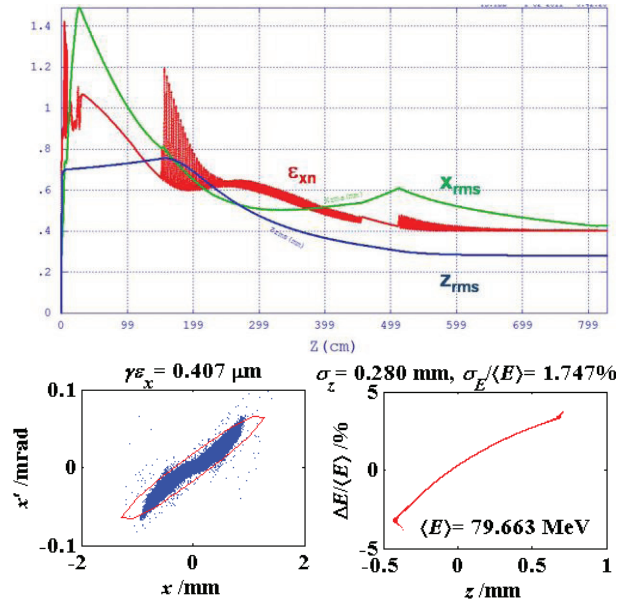| Energy	(MeV)	80-720
Bunch charge	(pC)	25-400
Bunch length	(μm)	100-400
$\varepsilon_{n\_x,y}$	(mm-mrad)	0.2-0.6
Bunch Energy spread	(%)	0.04-0.1
Focal spot size	(μm)	> 10
# bunches in the train		$\leq$32
Bunch separation	(nsec)	16
energy variation along the train		0.1 %
Energy jitter shot-to-shot		0.1 %
Emittance dilution due to beam breakup		< 10%
Time arrival jitter	(psec)	< 0.5
Pointing jitter	(μm)	1

Figure 3: TSTEP output for the reference working point, Q=250pC: Evolution of emittance, transverse and longitudinal envelopes in the S-band photo-injector (top), transverse (bottom left) and longitudinal (bottom right) phase space at the photo-injector exit.

between the electron beam and a high power laser is meant to produce the gamma-ray photon beam via Compton back-scattering. In Fig. 2 a schematic layout of the machine is reported. The repetition rate of the machine is 100 Hz, however within the RF pulse, whose duration is about 450 nsec, up to 30 electron bunches will be accelerated, each one carrying 250 pC of charge, separated by 15 nsec, raising the effective repetition rate of the electron bunches up to 3 kHz.

The Photoinjector

The SPARC-like photoinjector consists in a 1.6 cell RF gun equipped with a copper photocathode and an emittance compensation solenoid, followed by two S.band TW accelerating sections (SLAC-type). A gentle (compression factor <3) velocity bunching, as routinely done at SPARC, is applied in the first accelerating section, that is equipped with a 0.4 T solenoid in order to inject, without emittance degradation, a short enough electron beam in the C-band following linac, and reduce the final energy spread to the desired value. In Fig, 3 the simulations results obtained with the TSTEP [14] code, an updated version of the macroparticle code PARMELA [15], are shown from the photocathode down to the photoinjector exit; a thermal emittance of 0.9 mm-mrad/(mm rms) is comsidered [10]. The considered

accelerating gradient in the S-band accelerating sections is 21 MV/m, typically employed during SPARC operation, although a gradient of 23-25 MV/m could be reached. A number of 40K macroparticles has been used to simulate the "reference" working point based on a 250 pC electron beam.

The RF C-band Linac

The RF Linac that follows the photoinjector is made of twelve C-band, 1.8 m long, accelerating sections, which design has been developed at LNF [17], operating at 5.7 GHz with an average accelerating gradient E_{acc}=33 MV/m, for a maximum final energy of about 800 MeV on crest. The beam loading effect and the Beam Break UP (BBU) instability have been extensively studied to guarantee the multibunch operation feasibility [9,17]. In particular the beam loading in the structures will be compensated with a modulation of the input power to maintain the required energy spread along the bunch train.
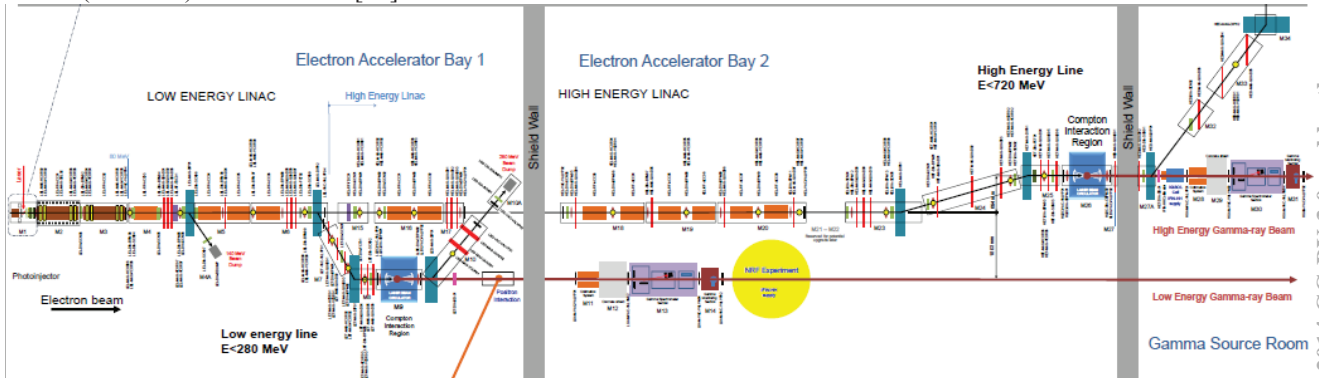
Figure 2: ELI-NP Gamma Beam System schematic layout [9].

For the BBU a strong damping solution has been adopted for which each cell of the structure has four waveguides that allows the excited HOMs to propagate and dissipate into loads [18], see Fig. 4.
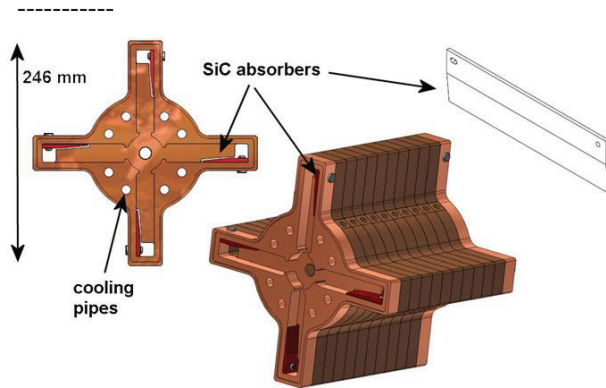

Figure 4: Detail of the TW cell with absorbers.

In the machine layout two beamlines are provided to deliver the electron beam at the two Compton Interaction Points (IP's): one at E=280 MeV and one at E=600 MeV. After the photoinjector a first linac section, Linac1, with 4 C-band accelerating structures brings the electron beam energy up to a maximum energy of 320 MeV on crest, followed by a dogleg DL1 that provides on right side an off axis deviation of about 180 cm. This branch delivers the electron beam to the low energy Compton IP avoiding in this way the bremsstrahlung radiation contribution. The straight extension downstream the Linac1 exit brings the electron beam at the entrance of the Linac2 where the beam energy can be raised up to a maximum energy of 800 MeV on crest. After the Linac2 a second dogleg DL2 delivers the beam to the high energy Compton IP with an opposite off axis deviation of 70 cm. The downstream dogleg DL3 guides the electron beam to the high energy dumper located outside the accelerator bunker. At each dogleg exit a quadrupole triplet provides the electron beam transverse focusing for the interaction with the laser.
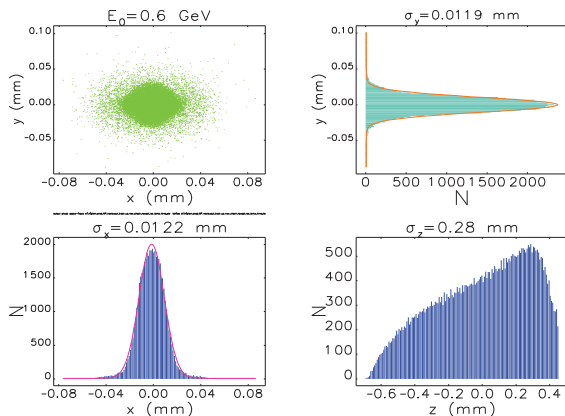

Figure 5: Transverse beam size and longitudinal distribution for the reference working point electron beam at the high energy IP, as obtained with 40kp Elegant tracking.
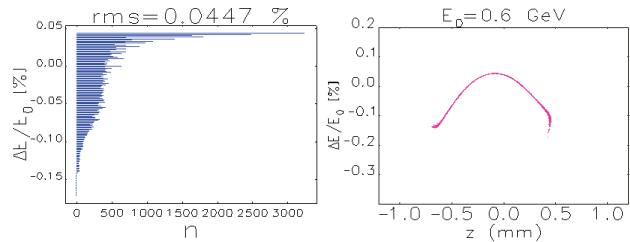

Figure 6: Energy spread (left) and energy distribution (right) of the reference working point electron beam at the high energy interaction point.

With the Elegant code [19] the simulated beam coming from the photoinjector has been tracked through the Linac1 and 2 down to the low and high energy IP's: in Fig 5 and 6 the simulation results are shown as obtained for the transverse and longitudinal phase space of the 600 MeV electron beam at the high energy interaction point, in agreement with requirements of Table 2. The interaction has been simulated for this case with the CAIN code [20] obtaining 2.8×10^5 photons/shot, in the 0.5 % bw, within 88 mrad collimation angle.

CONCLUSIONS

The ELI-NP GBS RF Linac, has been designed to maximize the gamma ray source spectral density as strictly dependant on the 4D electron beam phase space density, $\eta = Q/\epsilon_n^2$, the common features with the high brightness electron beams expertise have been here discussed.

REFERENCES

[1] B. E. Carlsten, Nucl. Instr. Meth. Phys. Res., Sect. A **285**, 313 (1989).
[2] L. Serafini and J. B. Rosenzweig, Phys. Rev. E **55**, 7565 (1997).
[3] M. Ferrario et al., SLAC-PUB-8400.
[4] M. Ferrario et al., Phys. Rev. Lett. **99**, 234801 (2007)
[5] B. Aune and R. H. Miller, SLAC-PUB 2393, 1979.
[6] L. Serafini, M. Ferrario, AIP Conf. Proc. 581, 87 (2001).
[7] K. L. F. Bane et al., Phys. Rev. ST Accel. Beams 12, 030704 (2009).
[8] M. Ferrario et al., Phys. Rev. Lett. **104**, 054801 (2010)
[9] arXiv:1407.3669 [physics.acc-ph]
[10] A. Bacci et al ., Proc. of IPAC2011, p. 1461
[11] C. Vaccarezza et al., Proc. of IPAC2012, p. 1086
[12] V. Petrillo et al., Nucl. Instr. & Meth A, **693**, pp.109-116, (2012)
[13] T. Weitkamp et al., Optics Express 13, 6296 (2005).
[14] L.M. Young priv. comm.
[15] L. M. Young, LANL Report No. LA-UR-96-1835.
[17] D. Alesini et al., Proc. of IPAC2013, p. 2726
[18] D. Alesini et al., Proc. of IPAC2014, p. 3856
[19] M. Borland, "elegant: A Flexible SDDS-Compliant Code for Acc. Sim.", APS LS-287, September 2000
[20] http://www-acc-theory_kek.jp/members/cain (1985)